Electronic Supplementary Material (ESI) for Sensors & Diagnostics.

Supplementary Material

Laser-induced fabrication of gold nanoparticles onto paper substrates and their application on paper-based electroanalytical devices

Iana V. S. Arantes[a], Vanessa N. Ataíde[a], Wilson A. Ameku[a], Juliana L. M. Gongoni[a], Jéssica S. G. Selva[a], Helton P. Nogueira[a,b], Mauro Bertotti[a], Thiago R. L. C. Paixão[a,*].

[a]Department of Fundamental Chemistry, Institute of Chemistry, University of São Paulo, São Paulo, SP, 05508-000, Brazil

[b]Department of Physical Chemistry, Institute of Chemistry, University of Campinas, Campinas, SP, 13083-970, Brazil

*Corresponding Author

E-mail Address: trlcp@iq.usp.br

Phone: +55 11 30919150

S1. SECM characterization procedure

The Pt microelectrode was fabricated by sealing a 25 µm diameter platinum wire (99.99%, Goodfellow) inside a borosilicate glass capillary (length: 10 cm; OD: 1.0 mm; ID: 0.50 mm, Sutter Instruments), using a P-2000 Micropipette Puller (Sutter Instrument Company). The radius of the fabricated Pt microelectrode was calculated from the diffusion limiting current obtained by recording cyclic voltammograms in $[Fe(CN)_6]^{3-}$ solution (**Fig. S1-A**), and the value was found to be 10 µm. SECM was used to estimate the RG value of the microelectrode (RG = Rg/a, where Rg = radius of the insulating glass surrounding the tip; a = radius of the Pt fiber). An approach curve was recorded in a 0.1 mol L^{-1} KCl solution containing 10 mmol L^{-1} $[Fe(CN)_6]^{3-}$ using a silicon wafer as substrate (**Fig. S1-B**). After fitting the experimental data with theoretical equations, the RG was found to be 10.

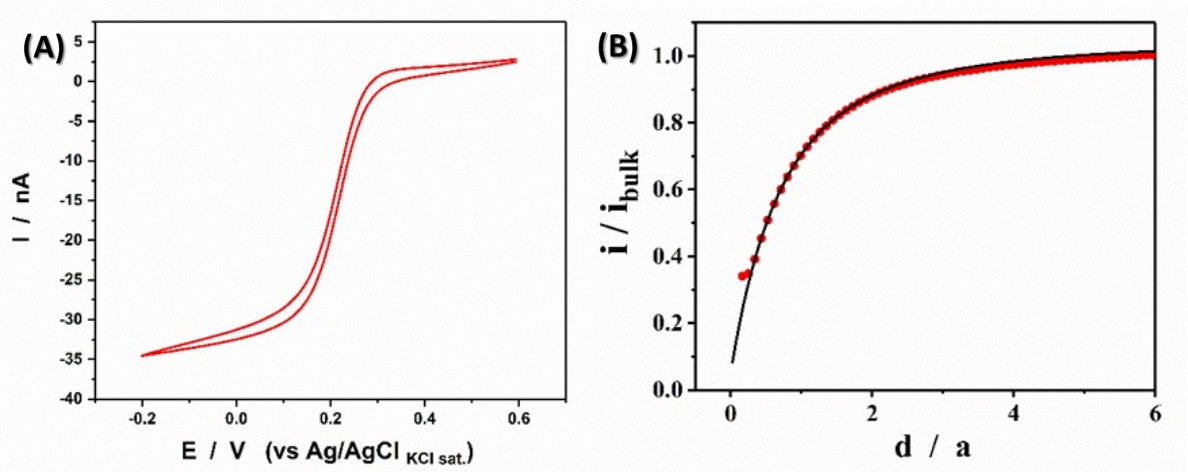

Fig. S1 - (A) Cyclic voltammogram recorded with a Pt UME in 10 mmol L^{-1} $[Fe(CN)_6]^{3-}$ in 0.1 mol L^{-1} KCl solution. Scan rate: 50 mV s^{-1}. **(B)** Approach curve recorded with the Pt UME (r = 10 µm) on a silicon wafer as an insulator substrate, where: (●) experimental data; (—) theoretical fit for an RG of 10.

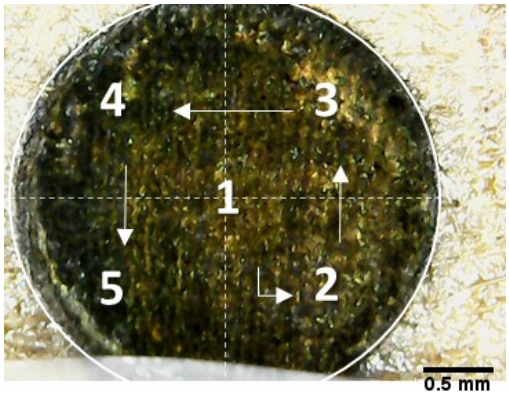

Fig. S2 - Optical image of the LSAu-ePAD showing the 5 probed locations during the SECM characterization.

S2. BIA-ePAD operation

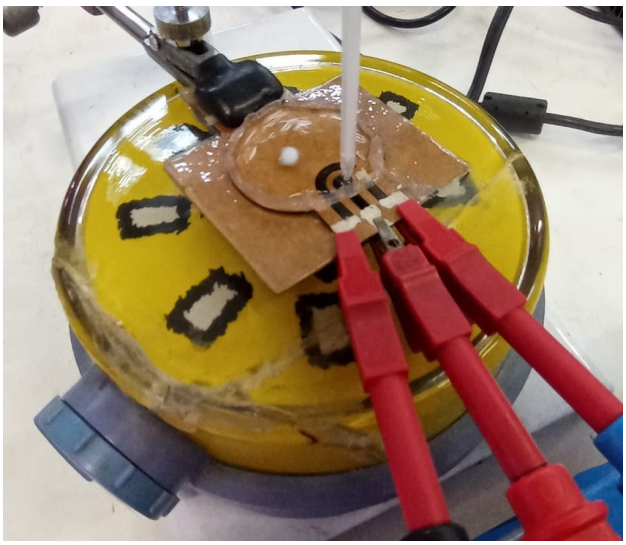

Fig. S3 – Image of the LSAu-ePAD operating in the BIA configuration.

S3. LSAu-ePAD optimization

Table S1 – Optimization of the CO_2 laser parameters for kraft paper carbonization, based on the sheet resistance (n=3).

Scan rate: 10 mm s^{-1} **Z-distance: 11 mm**		**Scan rate: 10 mm s^{-1}** **Power: 8 %**		**Z-distance: 11 mm** **Power: 8 %**	
Power (%)	**Resistance (Ω)**	**Z-distance (mm)**	**Resistance (Ω)**	**Scan rate (mm s^{-1})**	**Resistance (Ω)**
7.0	1.5k ± 0.3k	8	190 ± 20	6	430 ± 15
7.5	640 ± 26	10	295 ± 38	8	460 ± 23
8.0	405 ± 23	11	405 ± 23	10	405 ± 23
8.5	280 ± 21	12	300 ± 18	12	440 ± 50
9.0	170 ± 36	15	325 ± 35	15	980 ± 180

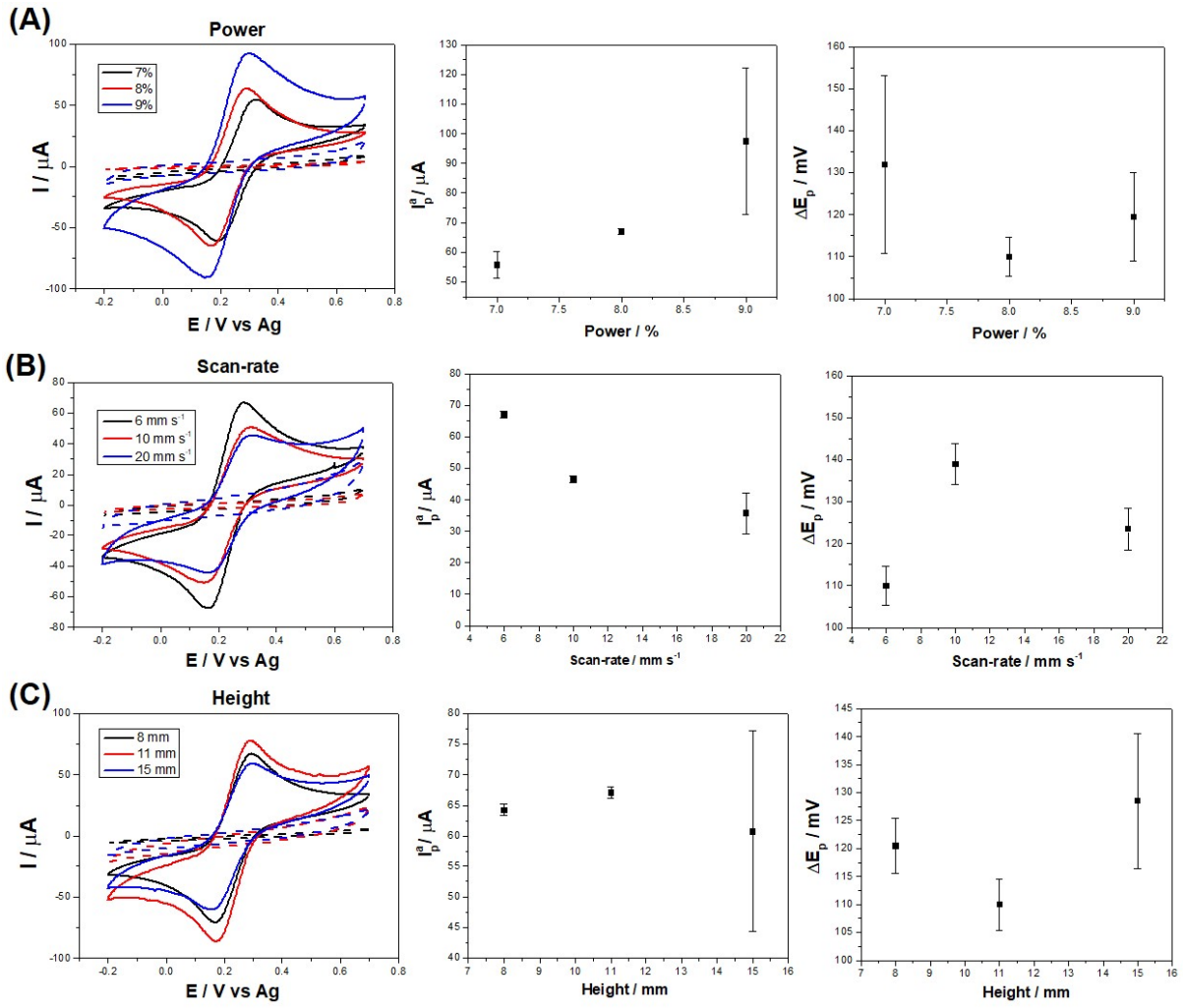

Fig. S4 – Optimization of the CO_2 laser parameters: **(A)** laser power, **(B)** scan rate, and **(C)** height for the thermal treatment of the Au/C surface (n=3), based on the anodic peak currents (Ip^a) and the peak-to-peak separation (ΔEp) obtained from CVs of 5 mmol L^{-1} $[Fe(CN)_6]^{3-/4-}$ in 1 mol L^{-1} KCl. Scan rate: 20 mV s^{-1}. $HAuCl_4$ volume and concentration: 20 µL of 20 mmol L^{-1}. Fixed parameters in **(A)**: 10 mm s^{-1} scan rate and 11 mm height, **(B)**: 8% laser power and 11 mm height, and **(C)**: 8% laser power and 10 mm s^{-1} scan rate.

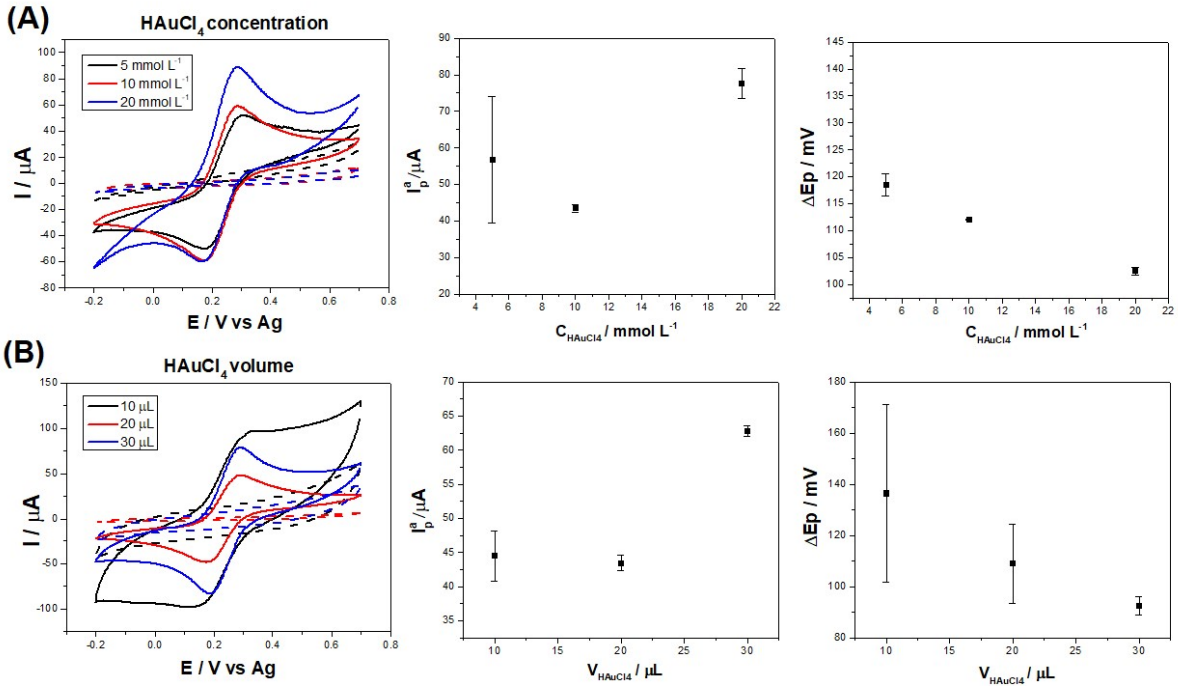

Fig. S5 – Optimization of the $HAuCl_4$ concentration **(A)** and volume **(B)** in the modification of the carbonized paper surface, based on the anodic peak currents (Ip^a) and the peak-to-peak separation (ΔEp) obtained from CVs of 5 mmol L^{-1} $[Fe(CN)_6]^{3-/4-}$ in 1 mol L^{-1} KCl. Scan rate: 20 mV s^{-1}. Fixed laser parameters: 8% laser power, 6 mm s^{-1} scan rate, and 11 mm height. $HAuCl_4$ volume in **(A)**: 20 µL, and $HAuCl_4$ concentration in **(B)**: 20 mmol L^{-1}.

S4. Morphological characterization

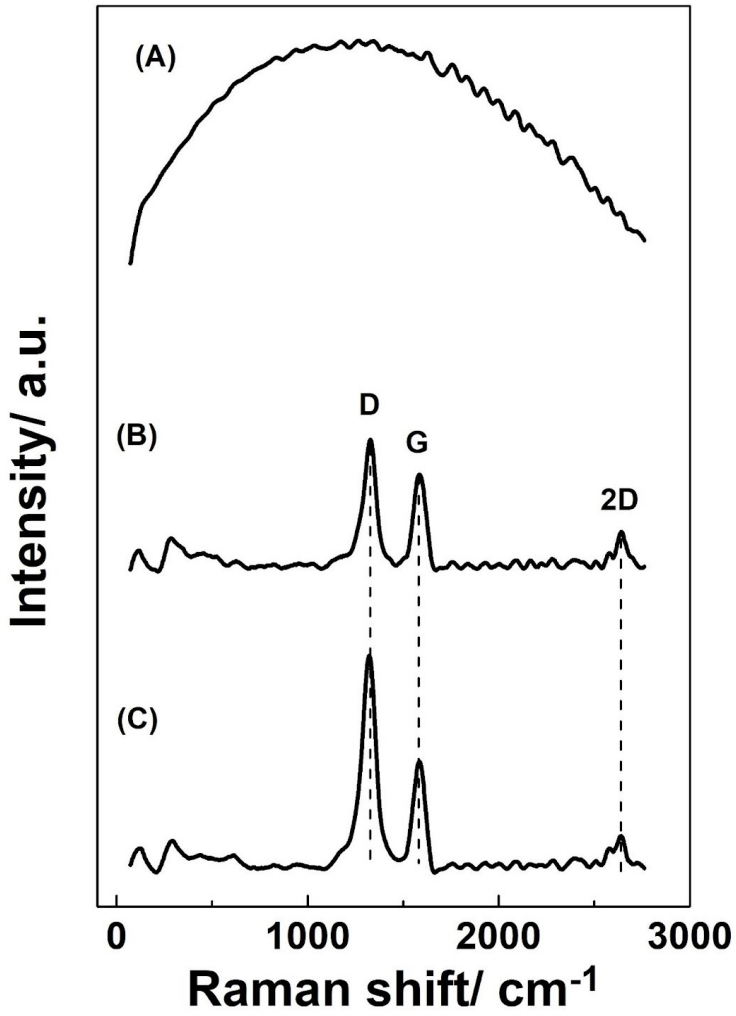

Fig. S6 – Raman spectra of the **(A)** bare kraft paper, **(B)** LS-ePAD, and **(C)** LSAu-ePAD.

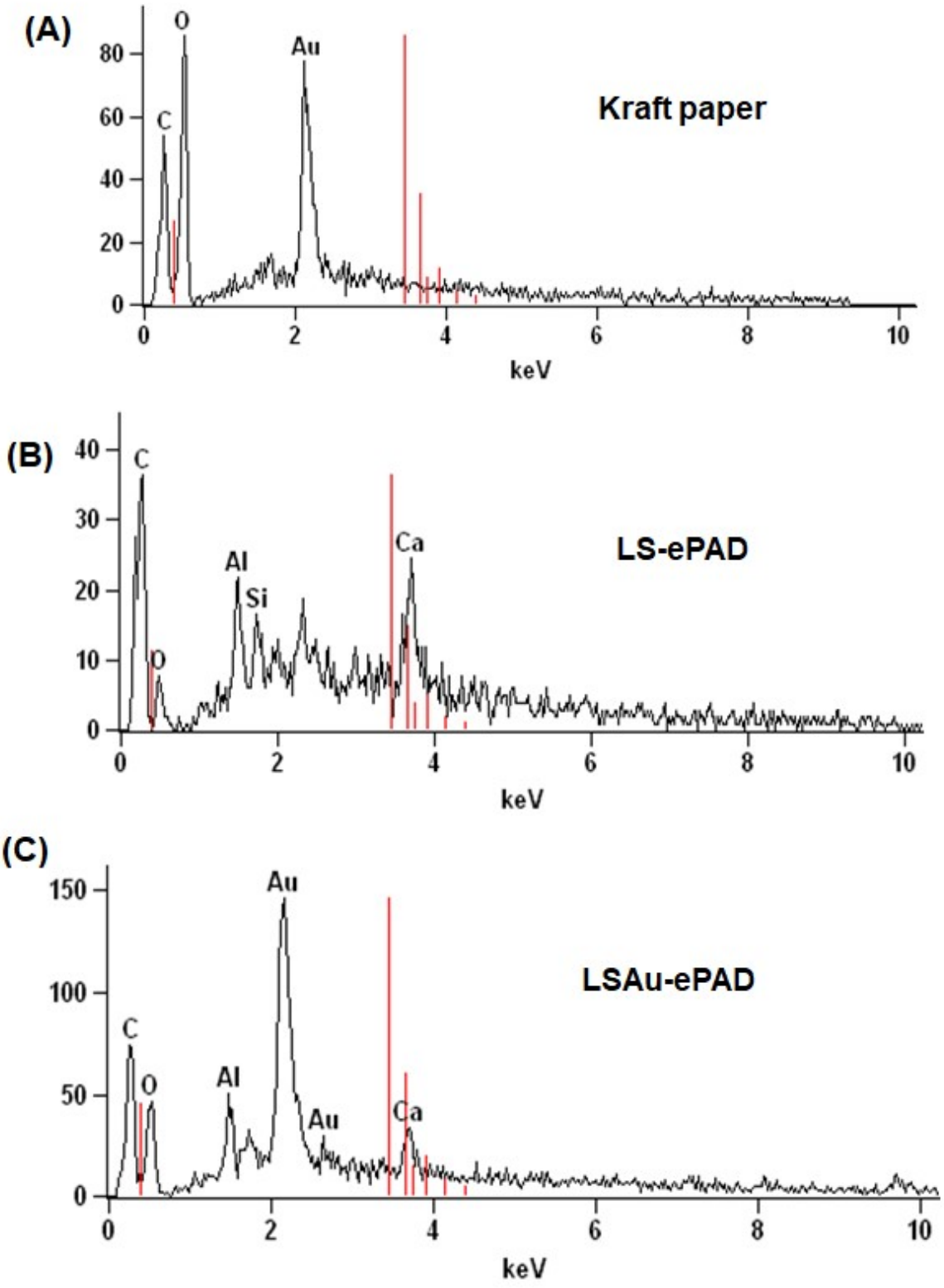

Fig. S7 - EDS analysis of the **(A)** bare kraft paper, **(B)** LS-ePAD, and **(C)** LSAu-ePAD.

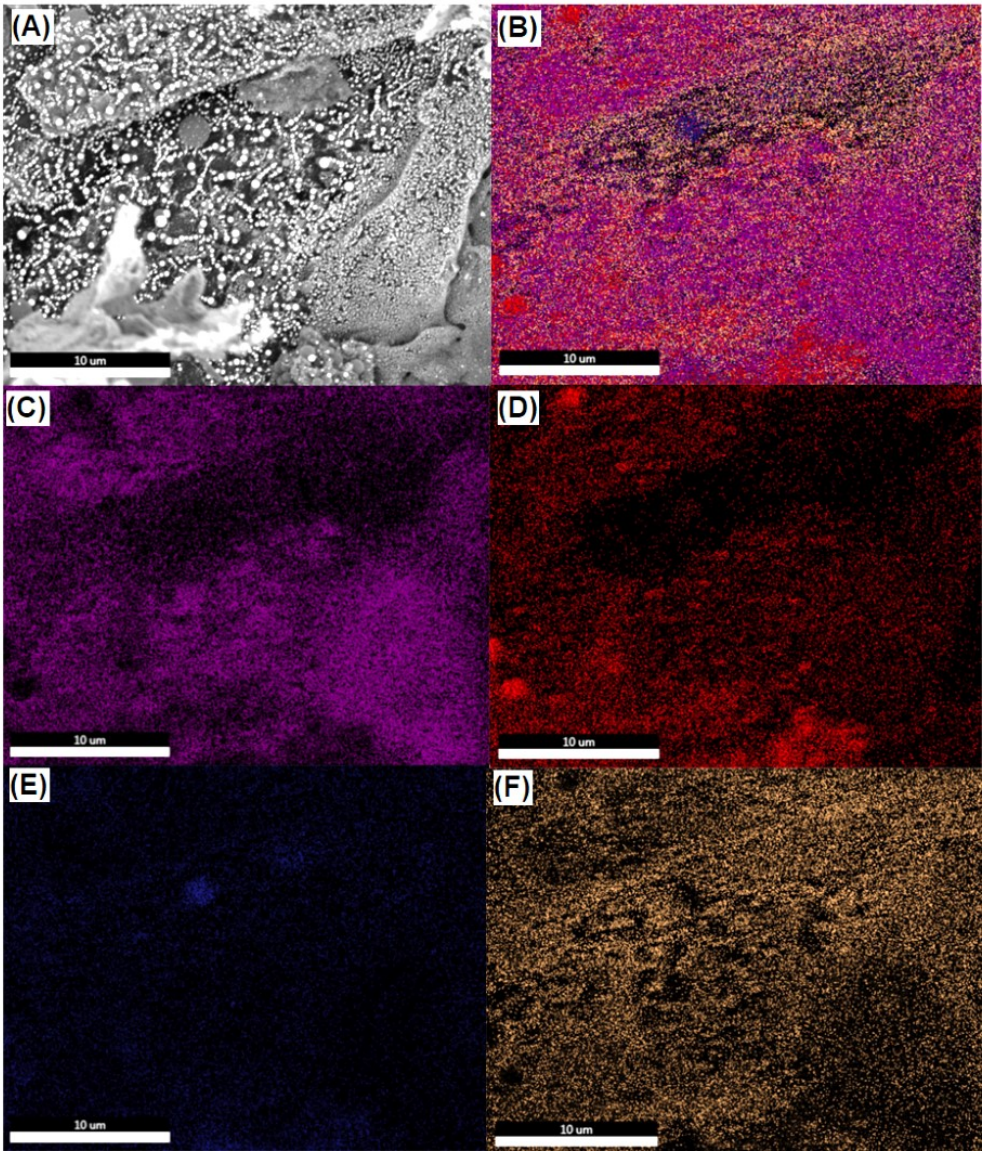

Fig. S8 – (A) SEM image of the LSAu-ePAD and the respective EDS elemental mapping showing **(B)** the element overlay of **(C)** carbon, **(D)** oxygen, **(E)** silicon, and **(F)** gold.

S5. Electrochemical characterization

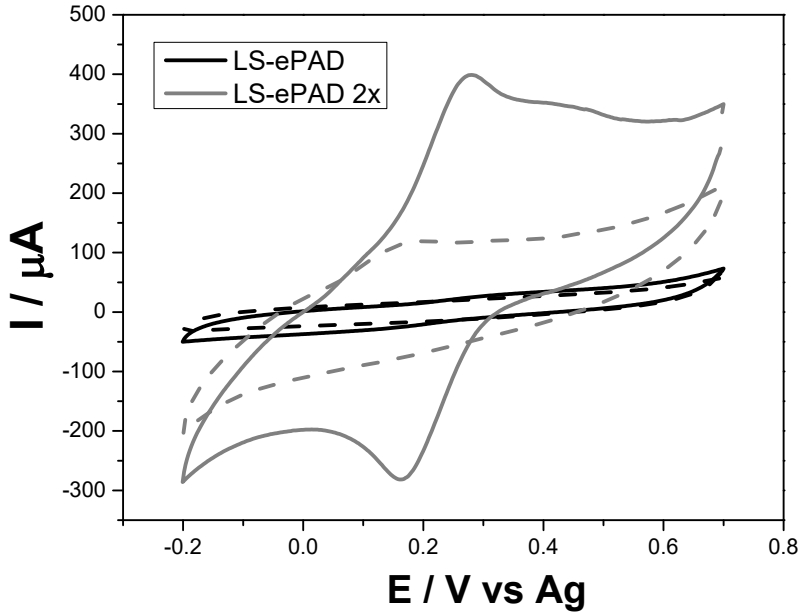

Fig. S9 - Cyclic voltammograms of 5 mmol L^{-1} $[Fe(CN)_6]^{3-/4-}$ (solid lines) in 1 mol L^{-1} KCl (dashed lines) recorded with the LS-ePADs with one (black color) and two (grey color) carbonization steps, without $HAuCl_4$ addition. Scan rate: 20 mV s^{-1}.

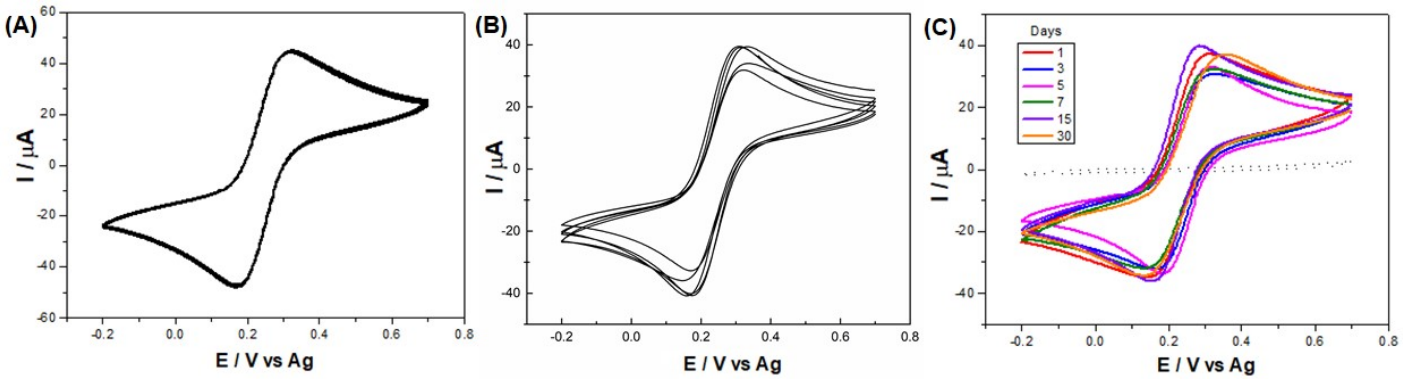

Fig. S10 – Cyclic voltammograms of 5 mmol L^{-1} $[Fe(CN)_6]^{3-/4-}$ in 1 mol L^{-1} KCl recorded with **(A)** the same LSAu-ePAD device (n=10) to attest the repeatability**; (B)** different devices fabricated in the same day (n=5) for reproducibility evaluation; and **(C)** different devices post 1, 3, 5, 7, 15, and 30 days of fabrication, to attest the Au modification stability over time in the LSAu-ePAD surface. Scan rate: 20 mV s^{-1}.

S6. SECM characterization results

Table S2 – Percentage of ferricyanide consumption on the surface device after polarization.

Device	1 (%)	2 (%)	3 (%)	4 (%)	5 (%)	Average (%)
LS-ePAD	83.6	71.9	75.3	51.6	50.8	66.6 ± 14.7
LSAu-ePAD	85.2	88.4	87.2	87.2	86.1	86.8 ± 1.2

S7. Hypochlorite detection

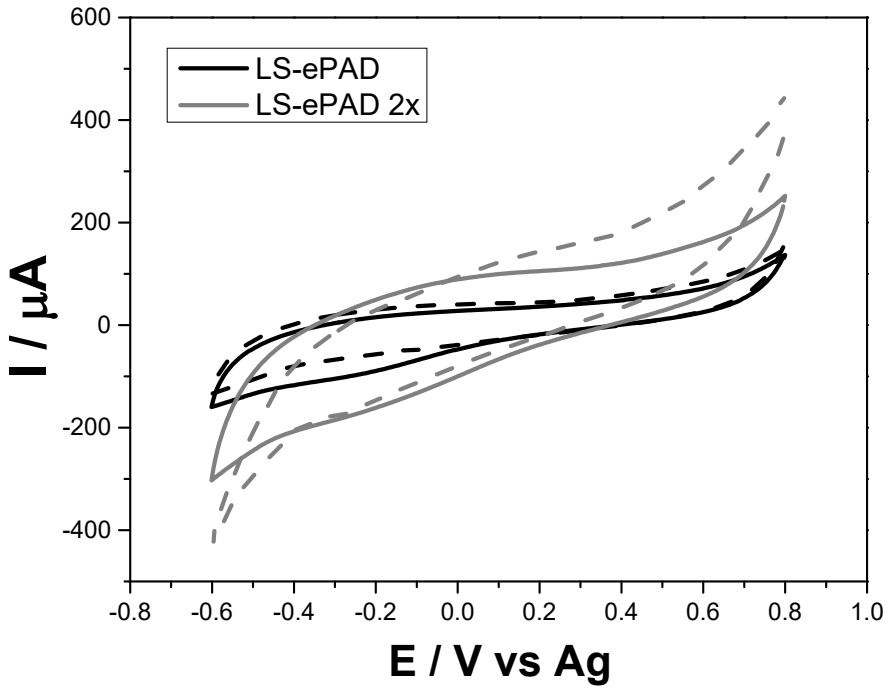

Fig. S11 – Cyclic voltammograms recorded with the LS-ePADs in 5 mmol L^{-1} NaClO (solid lines) in 0.04 mol L^{-1} BR buffer pH 8 (dashed lines) with one (black trace) and two (grey trace) carbonization steps, without $HAuCl_4$ addition. Scan rate: 50 mV s^{-1}.

S8. BIA-ePAD optimization parameters

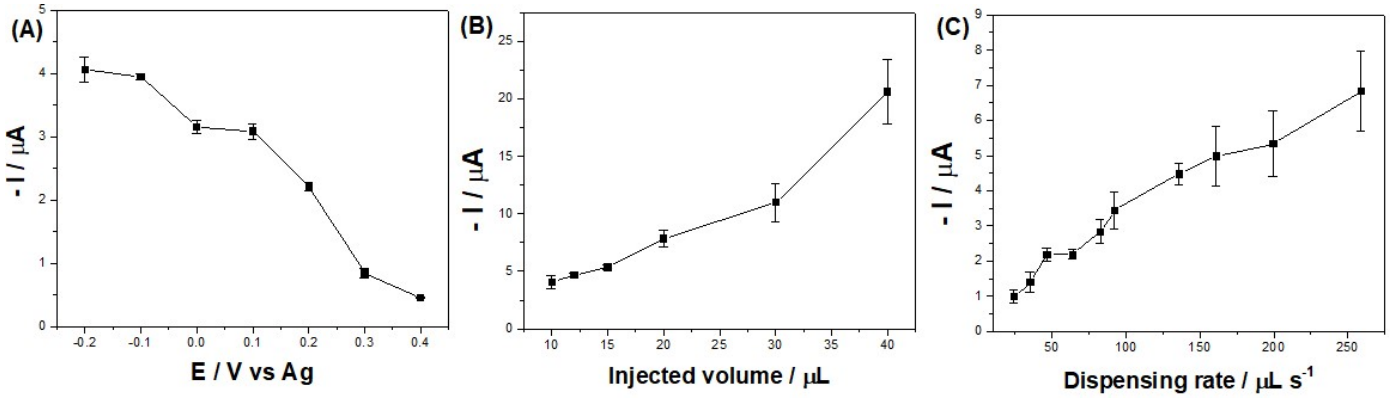

Fig. S12 – (A) Hydrodynamic voltammogram obtained from triplicate injections of 0.5 mmol L^{-1} NaClO in the BIA LSAu-ePAD at different potentials ranging from +0.4 to -0.2 V vs. Ag. Injected volume: 10 µL; Dispensing rate: 260 µL s^{-1}**. (B,C)** Amperometric current plots obtained from injections of 0.5 mmol L^{-1} NaClO by varying the **(B)** injected volume from 10 to 40 µL, with a fixed dispensing rate of 260 µL s^{-1}; and the **(C)** dispensing rate, from 25 to 260 µL s^{-1}, with a fixed volume of 10 µL. The electronic micropipette controlled both parameters. Applied potential: -0.2 V vs Ag. Supporting electrolyte: 0.04 mol L^{-1} BR buffer pH 8.

S9. Reproducibility of the BIA-ePAD

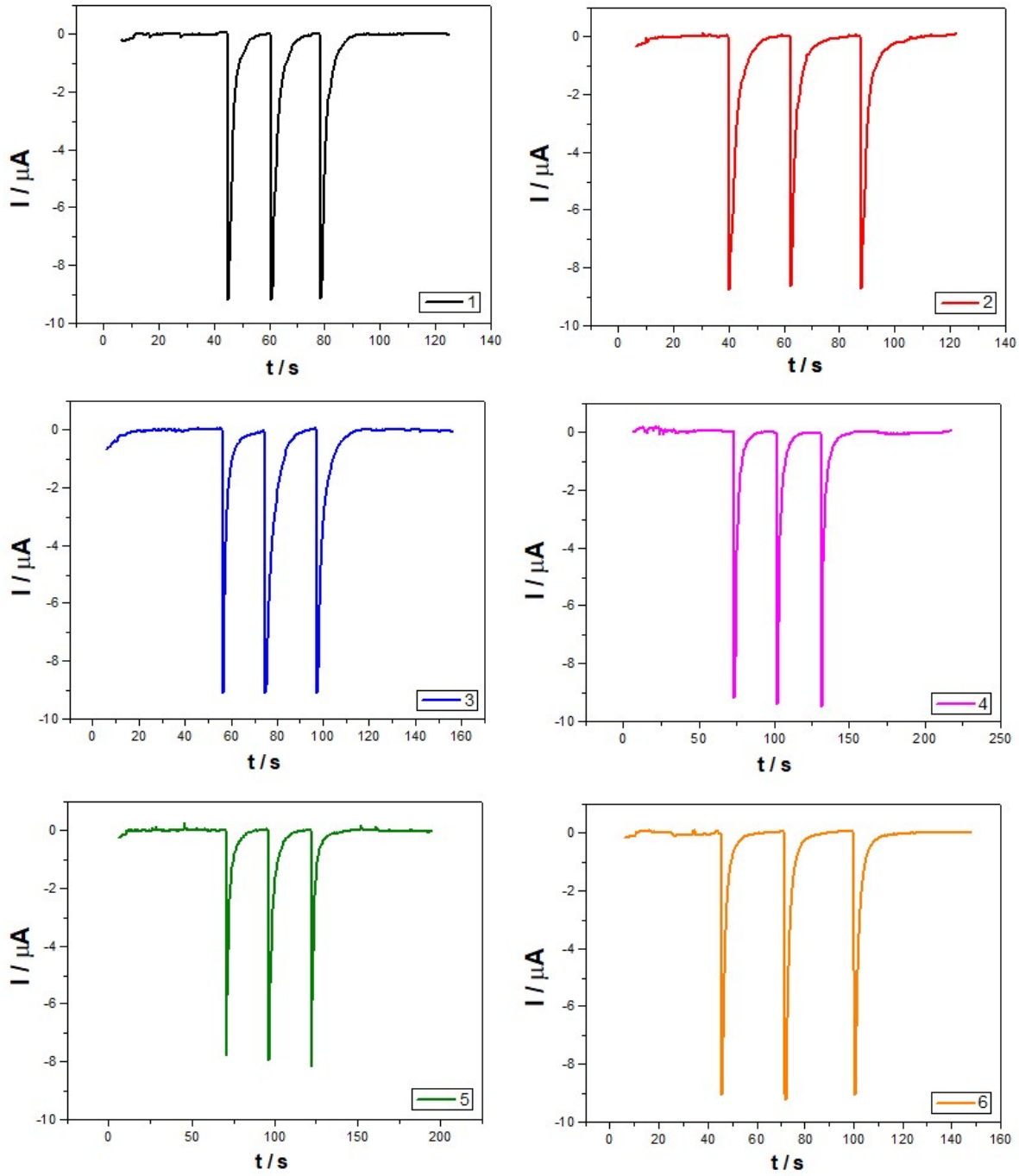

Fig. S13 - Reproducibility study for different fabricated BIA-ePADs obtained from injections of 0.5 mmol L^{-1} NaClO (RSD = 5.3%; n = 6). Applied potential: -0.2 V vs Ag; Injected volume: 20 µL; Dispensing rate: 135 µL s^{-1}; Supporting electrolyte: 0.04 mol L^{-1} BR buffer pH 8.

S10. Analytical application

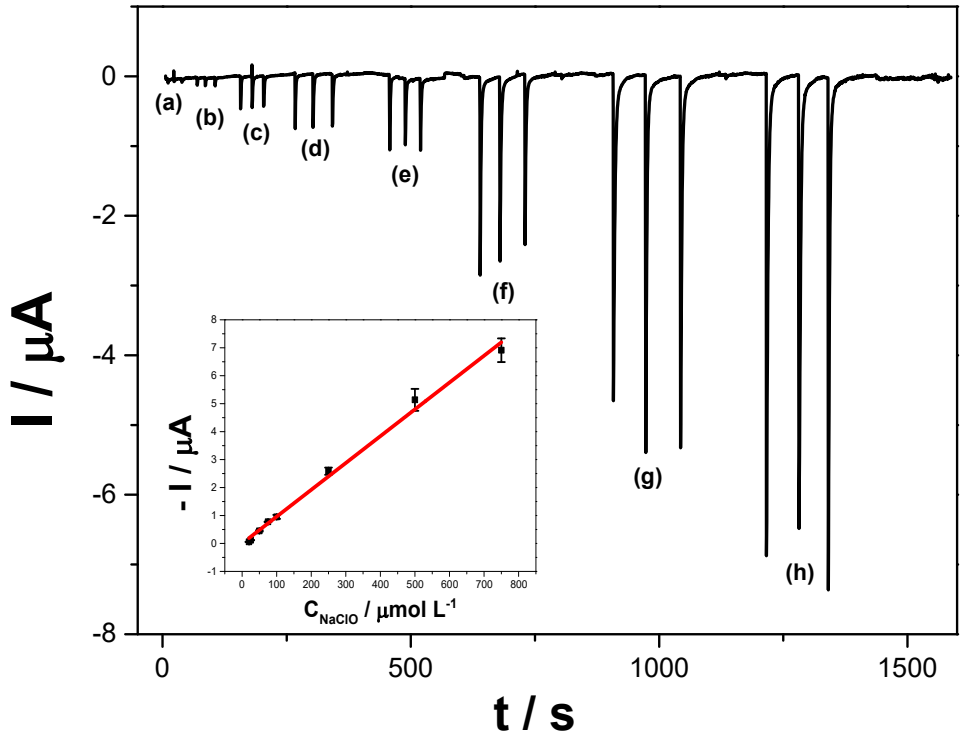

Fig. S14 - Amperometric responses obtained from triplicate injections of NaClO in the BIA-ePAD for a linearity study with a concentration range from 20 to 750 µmol L^{-1} (a - h) and the respective calibration curve of the peak currents vs. NaClO concentration (insert). Applied potential: −0.2 V vs. Ag; Injected volume: 20 µL; Dispensing rate: 135 µL s^{-1}; Supporting electrolyte: 0.04 mol L^{-1} BR buffer pH 8.

Table S3 - Analytical characteristics obtained for the amperometric measurements in the BIA-ePAD compared to other electrochemical devices presented in the literature for NaClO detection.

Electrode	Detection method	LR (ppm)	Sensitivity ($\mu A\ ppm^{-1}$)	LOD (ppm)	Ref.
Au disk electrode	DPV	1 - 5	0.0818	0.04	[1]
Multiwall carbon nanotubes composite electrode	FIA-AMP	0.02 - 4	0.1460	0.02	[2]
Pencil lead graphite-based electrode modified w/ ammonium carbamate	AMP	0 - 6	0.3020	-	[3]
Graphite screen-printed electrode modified w/ carbon black	AMP	0.05 - 200	0.3200	0.01	[4]
Au interdigitated microelectrode arrays	LSV	0 – 4.5	0.0004	0.01	[5]
Au thin film electrode	AMP	0 - 6	0.3270	-	[6]
Laser-scribed paper-based electrode modified w/ AuNPs	BIA-AMP	1.5 - 56	0.2280	0.50	This work

LR – Linear range. **DPV –** Differencial pulse voltammetry. **FIA –** Flow injection analysis. **AMP –** Amperometric. **LSV –** Linear sweep voltammetry.

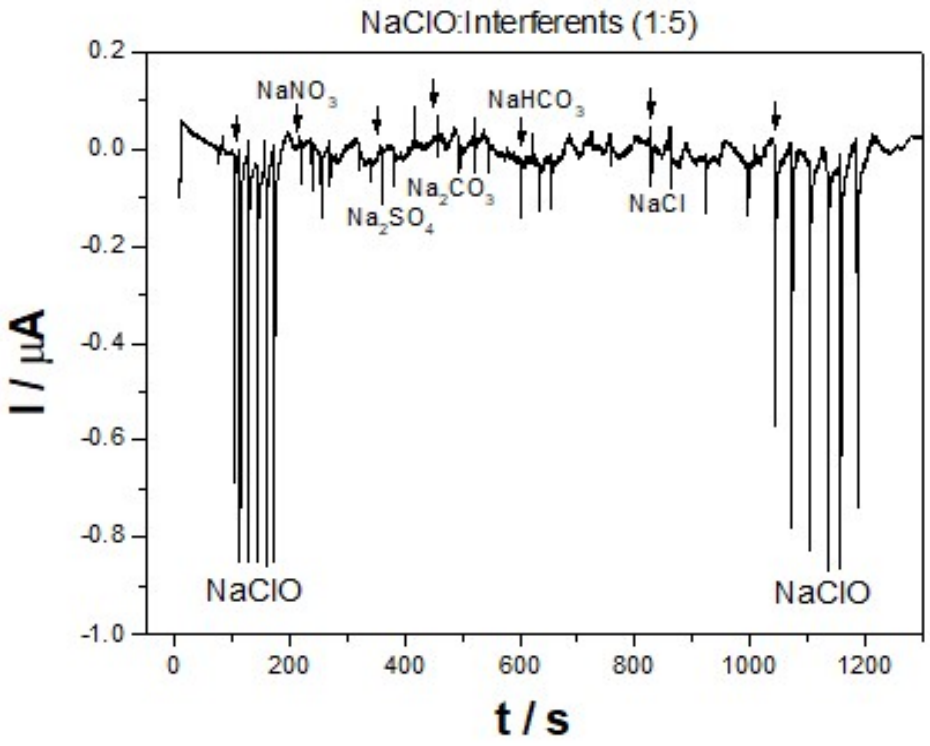

Fig. S15 – Amperogram responses corresponding to successive injections of 100 µmol L^{-1} NaClO and the most common interferents found in swimming pool waters, *i.e.*, Na_2SO_4, Na_2CO_3, $NaHCO_3$, and NaCl (500 µmol L^{-1}). Applied potential: -0.2 V vs Ag; Injected volume: 20 µL; Dispensing rate: 135 µL s^{-1}; Supporting electrolyte: 0.04 mol L^{-1} BR buffer pH 8.

REFERENCES

[1] S. Saputro, K. Takehara, K. Yoshimura, S. Matsuoka, Narsito, Differential pulse voltammetric determination of free chlorine for water disinfection process, Electroanalysis. 22 (2010) 2765–2768. https://doi.org/10.1002/elan.201000322.

[2] R. Olivé-Monllau, A. Pereira, J. Bartrolí, M. Baeza, F. Céspedes, Highly sensitive CNT composite amperometric sensors integrated in an automated flow system for the determination of free chlorine in waters, Talanta. 81 (2010) 1593–1598. https://doi.org/10.1016/J.TALANTA.2010.03.008.

[3] S. Pan, M.J. Deen, R. Ghosh, Low-Cost Graphite-Based Free Chlorine Sensor, Anal. Chem. 87 (2015) 10734–10737. https://doi.org/10.1021/acs.analchem.5b03164.

[4] M.R. Tomei, F. Arduini, D. Neagu, D. Moscone, Carbon black-based disposable sensor for an on-site detection of free chlorine in swimming pool water, Talanta. 189 (2018) 262–267. https://doi.org/10.1016/j.talanta.2018.07.005.

[5] I. Seymour, B. O'Sullivan, P. Lovera, J.F. Rohan, A. O'Riordan, Electrochemical

Detection of Free-Chlorine in Water Samples Facilitated by in-situ pH Control using Interdigitated Microelectrodes, ChemRxiv. 325 (2020). https://doi.org/10.26434/chemrxiv.11898126.v1.

[6] A.U. Alam, D. Clyne, W. Lush, M.J. Deen, A reusable, reagent-less free chlorine sensor using gold thin film electrode, Analyst. 146 (2021) 2626–2631. https://doi.org/10.1039/d1an00038a.